Inhalation Toxicology, 20:227–243, 2008

ISSN: 0895-8378 print / 1091-7691 online
DOI: 10.1080/08958370701864235

informa
healthcare

Application of Physiological Computational Fluid Dynamics Models to Predict Interspecies Nasal Dosimetry of Inhaled Acrolein

Jeffry D. Schroeter, Julia S. Kimbell, and Elizabeth A. Gross
The Hamner Institutes for Health Sciences, Research Triangle Park, North Carolina, USA

Gabrielle A. Willson
EPL, Inc., Research Triangle Park, North Carolina, USA

David C. Dorman, Yu-Mei Tan, and Harvey J. Clewell III
The Hamner Institutes for Health Sciences, Research Triangle Park, North Carolina, USA

Acrolein is a highly soluble and reactive aldehyde and is a potent upper-respiratory-tract irritant. Acrolein-induced nasal lesions in rodents include olfactory epithelial atrophy and inflammation, epithelial hyperplasia, and squamous metaplasia of the respiratory epithelium. Nasal uptake of inhaled acrolein in rats is moderate to high, and depends on inspiratory flow rate, exposure duration, and concentration. In this study, anatomically accurate three-dimensional computational fluid dynamics (CFD) models were used to simulate steady-state inspiratory airflow and to quantitatively predict acrolein tissue dose in rat and human nasal passages. A multilayered epithelial structure was included in the CFD models to incorporate clearance of inhaled acrolein by diffusion, blood flow, and first-order and saturable metabolic pathways. Kinetic parameters for these pathways were initially estimated by fitting a pharmacokinetic model with a similar epithelial structure to time-averaged acrolein nasal extraction data and were then further adjusted using the CFD model. Predicted air:tissue flux from the rat nasal CFD model compared well with the distribution of acrolein-induced nasal lesions from a subchronic acrolein inhalation study. These correlations were used to estimate a tissue dose-based no-observed-adverse-effect level (NOAEL) for inhaled acrolein. A human nasal CFD model was used to extrapolate effects in laboratory animals to human exposure conditions on the basis of localized tissue dose and tissue responses. Assuming that equivalent tissue dose will induce similar effects across species, a NOAEL human equivalent concentration for inhaled acrolein was estimated to be 8 ppb.

Acrolein is a reactive aldehyde used as an intermediate in the production of acrylic acid and is also formed during combustion of organic materials. Human exposure to acrolein occurs primarily from tobacco smoke, gasoline and diesel exhaust, structural and forest fires, and partially combusted animal fats and vegetable oils (Beauchamp et al., 1985). Ambient indoor air concentrations are typically less than 12 ppb (ATSDR, 1990), but exposure concentrations can be much higher near fires or secondhand cigarette smoke (Brunnemann et al., 1990; Slaughter et al., 2004; Treitman et al., 1980).

As with many other aldehydes, acrolein is a potent respiratory-tract irritant, causing respiratory depression and hypersensitivity and altering mucociliary clearance in rodents (Beauchamp et al., 1985; Morris, 1996). Acrolein is highly soluble and reactive and produces cytotoxicity at the site of initial contact upon inhalation, thereby making the nasal passages an important target site. Inhaled acrolein reacts readily with sulfhydryls in nasal mucosa and has been shown to rapidly deplete rat nasal glutathione (Lam et al., 1985). Acrolein also initiates cell proliferation in the rat respiratory tract (Roemer et al., 1993). Acrolein-induced nasal pathology in rodents includes olfactory epithelial inflammation, olfactory neuronal loss, and inflammation, hyperplasia, and squamous metaplasia of the respiratory epithelium (Buckley et al., 1984; Cassee et al., 1996; Feron et al., 1978; Dorman et al., 2008). Nasal

Received 10 July 2007; accepted 2 November 2007.

The authors thank Dr. John Morris for research discussions and Drs. Guilherme Garcia and Melvin Andersen for their critical review of this article. This project was sponsored and funded by the American Forest and Paper Association.

Address correspondence to Jeffry D. Schroeter, PhD, The Hamner Institutes for Health Sciences, 6 Davis Drive, PO Box 12137, Research Triangle Park, NC 27709-2137, USA. E-mail: jschroeter@thehamner.org

extraction of inhaled acrolein in rats is moderate to high and is flow rate and concentration dependent, with uptake decreasing as exposure concentration increases, suggestive of saturable metabolic or reactive processes in nasal tissue (Morris, 1996; Struve et al., 2008).

In this study, anatomically accurate three-dimensional (3D) computational fluid dynamics (CFD) models of rat and human nasal passages were developed to predict interspecies nasal dosimetry of inhaled acrolein. Regional dose depends on airflow characteristics, exposure concentration, and the absorption properties of the nasal lining. Therefore, a multilayer epithelial structure lining the airway lumen was incorporated into the nasal CFD models to simulate acrolein disposition from the air:mucus interface throughout the epithelial lining. Clearance from the air phase was governed by air- and tissue-phase diffusion, solubility, blood perfusion, and other first-order and saturable clearance mechanisms in nasal epithelium. Inclusion of epithelial layers lining the nasal passages has been used in previous hybrid models combining CFD and physiologically based pharmacokinetic (PBPK) models to predict dosimetry of inhaled gases in rat and human nasal passages (Plowchalk et al., 1997; Frederick et al., 1998; Bogdanffy et al., 1999; Sarangapani et al., 2004), and more recently was used in nasal CFD models to predict dosimetry of inhaled hydrogen sulfide (Schroeter et al., 2006a, 2006b).

Dorman et al. (2008) recently conducted a subchronic acrolein inhalation study in adult male F344 rats. Nasal histopathology was evaluated at multiple sections in the nose and no-observed-adverse-effect levels (NOAELs) of 0.2 ppm and 0.6 ppm were identified for respiratory and olfactory epithelial pathology, respectively. In the present study, flux predictions from the rat CFD model at those histologic sites were used to establish a correlation between regions of high tissue dose and lesion incidence to estimate a tissue-dose-based NOAEL for acrolein-induced nasal lesions in rats. A NOAEL human equivalent concentration ($NOAEL_{[HEC]}$) was then derived using acrolein flux predictions calculated from the human nasal CFD model, assuming that equal tissue doses will invoke similar responses in rats and humans. This $NOAEL_{[HEC]}$ value can be used to establish a revised estimate of an inhalation reference concentration (RfC) for acrolein that is based on quantitative tissue dose estimates rather than on default dosimetric assumptions for interspecies extrapolation.

METHODS

CFD models of the rat and human nasal passages have been previously developed and include details of species-specific airflow patterns (Kimbell et al., 1997a; Subramaniam et al., 1998). This section discusses (1) the modification of these models to include an epithelial architecture describing tissue-phase mass transfer of inhaled acrolein, (2) the joint use of pharmacokinetic and CFD models to estimate kinetic parameters, and (3) use of the rat nasal CFD model to predict air:tissue flux at specific sites used for histopathological evaluation of inhaled acrolein.

Development of Physiological Computational Fluid Dynamics Models

Nasal Airflow Models

Airflow in the rat nasal passages was simulated in an anatomically accurate 3D reconstruction of the right nasal passages of a mature F344 rat from tracings of serial histological cross sections (Kimbell et al., 1997a). Human nasal airflow simulations were conducted in an anatomically accurate 3D model derived from magnetic resonance imaging (MRI) scan tracings of the nasal passages of a healthy adult male (Subramaniam et al., 1998). Computational meshes for these nasal CFD models consisted of structured hexahedral elements resulting in approximately 144,000 and 156,000 nodes for the rat and human, respectively. A no-slip (i.e., zero velocity) boundary condition was imposed on all epithelial surfaces, a stress-free condition was imposed at the outlet, and a uniform velocity profile was defined at the nostril(s). Steady-state inspiratory airflow was simulated by solving the viscous incompressible Navier–Stokes equations with the finite-element method using FIDAP (Fluent, Inc., Lebanon, NH). Simulated airflow rates used in this study are described later.

Gas Uptake Boundary Conditions

The absorption rate of inhaled acrolein at nasal airway walls was assumed to be proportional to the concentration of acrolein in the boundary layer of the air phase adjacent to the airway walls (C_{air}). This form of boundary condition is written:

$$\text{flux} = h \cdot C_{air} \quad [1]$$

where h is referred to as an air-phase mass transfer coefficient. The mass transfer coefficient was determined separately for non-mucus-coated squamous epithelium in the nasal vestibule, and mucus-coated respiratory, transitional, and olfactory epithelium throughout the rest of the nose of each species.

The nasal vestibule of rats and humans is comprised of squamous epithelium (Figure 1), which lacks the moist mucus layer lining the other epithelial types and histologically resembles skin. Acrolein is similar to formaldehyde in that both chemicals are highly soluble and reactive and are potent respiratory-tract irritants. Neither chemical has been shown to induce lesions in squamous epithelium, possibly indicating lower absorption rates than in the rest of the nose (Kimbell et al., 1997b).

A mass transfer coefficient for acrolein uptake by squamous epithelium in the rat and human nose was derived using an approach similar to that undertaken with formaldehyde (Kimbell et al., 2001b). In this approach, a tissue layer consisting of squamous epithelium was assumed to line the nasal vestibule. Assuming that mass transfer throughout this tissue occurs only by molecular diffusion (i.e., no chemical reaction is assumed and solubility is ignored due to the lack of mucus), the flux of

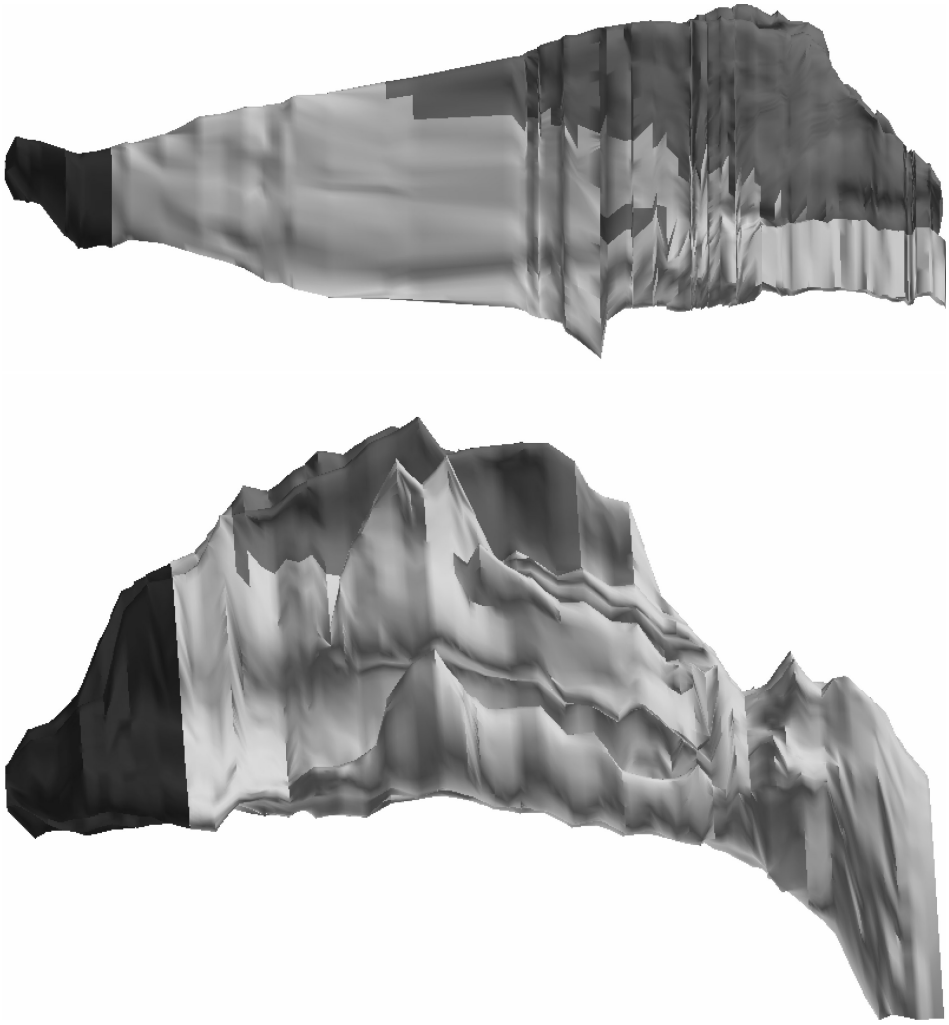

FIG. 1. CFD models of the rat (top) and human (bottom) nasal passages: squamous epithelium (black), respiratory/transitional epithelium (light gray), olfactory epithelium (dark gray). The nostrils are to the left, and the nasopharynx is to the right. The view of the rat CFD model shows the septal side of the right nasal passages.

acrolein into nasal tissue from the air phase can be written as:

$$\text{squamous flux} = \frac{D_s \cdot P_{s:a} \cdot C_{air}}{L_s} \quad [2]$$

where D_s is the diffusivity of acrolein in skin, $P_{s:a}$ is the skin:air partition coefficient, and L_s is the squamous epithelial thickness, assumed to be 20 μm. Under the equilibrium assumption at the air:tissue interface, flux from the air phase [Eq. (1)] can be equated with flux into tissue [Eq. (2)], yielding an equation for a mass transfer coefficient on squamous epithelium:

$$K_s = \frac{D_s \cdot P_{s:a}}{L_s}$$

The dermal diffusivity (D_s) and skin:air partition coefficient ($P_{s:a}$) of acrolein were estimated by scaling the corresponding values for formaldehyde based on the differences in water diffusivity and water:air partition coefficient between the two gases as follows. Formaldehyde is more diffusive than acrolein, with water diffusion rates of 1.98×10^{-5} cm^2/s versus 1.22×10^{-5} cm^2/s, respectively, yielding a ratio of 1.6. Formaldehyde is much more soluble than acrolein, with a water:air partition coefficient (Henry's law constant) of 72,464 for formaldehyde versus 200 for acrolein (Risk Assessment Information System, http://rais.ornl.gov, accessed May 2007), yielding a ratio of 362. We note that the water:air partition coefficient used here is higher than the value of 88 estimated by Morris (1996) and used later in this study because, for scaling consistency, we chose to take both the acrolein and formaldehyde values from the same source.

Kimbell et al. (2001b) assumed that absorption rates of inhaled formaldehyde on squamous epithelium were similar to uptake rates through human epidermal tissue (Loden, 1986). Using a resorption rate of 0.0166 mg/cm^2/h, they estimated the product of formaldehyde skin diffusivity and skin:air partition coefficient to be 1.13×10^{-8} cm^2/s. Scaling this value for acrolein

TABLE 1
Parameter values used in the rat and human nasal CFD models

Parameter	Rat	Human	Source
Body weight (kg)	0.315	72	Kimbell et al. (1997), Subramaniam et al. (1998)
Cardiac output (CO) (ml/min)	99	5200	Brown et al. (1997)
Nasal blood flow (% of CO)	0.01	0.01	Frederick et al. (1998)
Inhalation minute volume (ml/min)	217	6900	U. S. EPA (1994)
Nasal surface areas (cm^2)			
Total	18.2	247.4	Calculated from nasal CFD models
Squamous	0.8	20.2	(Kimbell et al., 1997a;
Respiratory	10.6	203.9	Subramaniam et al., 1998)
Olfactory	7.6	23.4	
Mucus layer thickness (μm)	10	20	Morris (1993), Sarangapani et al. (2004)
Epithelial layer thickness (μm)			Morris (1993), Frederick et al. (1998)
Respiratory	30	50	
Olfactory	60	50	
Submucosal layer thickness (μm)			Morris (1993), Plowchalk et al. (1997)
Olfactory	20	20	
Respiratory	20	20	
Acrolein water:air partition coefficient	88	88	Morris (1996)
Acrolein air diffusivity (cm^2/s)	0.105	0.105	The Risk Assessment Information System (http://rais.ornl.gov)
Acrolein water diffusivity (cm^2/sec)	1.22×10^{-5}	1.22×10^{-5}	The Risk Assessment Information System (http://rais.ornl.gov)

(i.e., scaled by 1.6×362), we estimated a mass transfer coefficient of $K_s = 7.1 \times 10^{-4}$ cm/s. This value was used in both the rat and human nasal CFD models for acrolein.

A two-tiered epithelial layer lining the air phase of the CFD model was implemented on wet squamous, respiratory, transitional, and olfactory epithelium (Figure A1). The former three epithelial types were assumed to be uniform and from here on are simply referred to as respiratory tissue. The epithelial structure consists of an epithelial cell layer, containing mucus and tissue layers lumped together, and a submucosal layer that includes clearance by blood perfusion. This tissue structure was previously proposed by Morris and colleagues (1993) for use in a PBPK model of nonreactive vapors in the rat nose, and similar structures have been implemented in numerous compartmental models of the nose (Plowchalk et al., 1997; Frederick et al., 1998; Andersen et al., 1999; Bogdanffy et al., 1999; Sarangapani et al., 2004). In this study, there was insufficient data available on acrolein clearance processes to distinguish the mucus layer from the epithelial cell layer. Likewise, there was no need to subdivide the epithelial layers into multicompartment tissue stacks as was done in the other compartmental models, due to similar acrolein clearance mechanisms throughout nasal tissue.

Mass transfer across mucus-coated epithelium was governed by acrolein diffusivity and solubility, and subsequent clearance in nasal tissues by saturable and nonsaturable pathways with additional blood flow clearance in the submucosal layer. The equations describing these convection-diffusion and reaction-diffusion processes are described in Appendix A. Flux into mucus-coated tissue is determined from the equilibrium assumption, where flux from the air phase is equal to flux into the tissue phase. Using Eq. (1), a numerical formula for the air-phase mass transfer coefficient was solved at every nodal point on the airway walls in the CFD model. The different clearance processes generate a concentration gradient from the air:mucus interface to the end of the submucosal layer, where zero concentration was assumed to reflect the direct reactivity and complete removal of acrolein by blood circulation.

Model parameters used in the nasal CFD models were taken from the aforementioned studies and are listed in Table 1. The mucus layer was set to be 10 μm thick in the rat and 20 μm thick in the human. Since the mucus layer was not treated as a separate compartment, these thicknesses were added to the epithelial cell layer thickness. Various tissue thicknesses for the rat have been reported, ranging from 20 to 40 μm for respiratory epithelial depth, and from 40 to 50 μm for olfactory epithelium (Morris, 1993; Frederick et al., 1998; Plowchalk et al., 1997; Sarangapani et al., 2004). We used a median value with a respiratory tissue thickness of 30 μm. Following Morris et al. (1993), olfactory epithelium in the rat was twice as thick as respiratory epithelium. Submucosal tissue was 20 μm thick (Morris, 1993; Plowchalk et al., 1997). Human epithelial thickness was 50 μm for respiratory and olfactory epithelium, and submucosal thickness was

20 μm. Nasal blood flow in the rat was 1% of cardiac output of 14,000 ml/h/kg scaled by body surface area (body weight to the 0.75 power) to a 315-g rat (Frederick et al., 1998; Brown et al., 1997). Human nasal blood flow was 1% of cardiac output of 5200 ml/min (Brown et al., 1997).

Parameter Estimation

The first-order rate constant, k_f, and the Michaelis–Menten parameters $V_{\max}$ and K_m governing clearance of inhaled acrolein in nasal tissue had to be estimated (see Appendix A). There are currently no efficient means of optimizing parameters with the CFD model due to the computationally intensive nature of the calculations and communication among several commercial software packages. Therefore, a pharmacokinetic (PK) model was developed that shared a similar model structure with the rat nasal CFD model to obtain an initial estimate of parameters. The PK model compartmentalized the air phase of the rat nose into squamous and nonsquamous epithelium, with an epithelial structure consisting of mucus/tissue and submucosal layers for the latter epithelial type (Figure B1). Mass balance equations for the three phases of the PK model are described in Appendix B.

Kinetic parameters were initially estimated by fitting predicted nasal extraction (NE) from the PK model with time-averaged acrolein NE from two in vivo studies (Morris, 1996; Struve et al., 2008). In these studies, the upper respiratory tract of anesthetized F344 rats was surgically isolated, and acrolein NE was measured under constant unidirectional flow. Morris (1996) used acrolein exposure concentrations of 0.9, 4.5, and 9.1 ppm with inspiratory flow rates of 50, 100, 200, and 300 ml/min (the data for the 100- and 300-ml/min flow rates were used in this study). Struve et al. (2008) used exposure concentrations of 0.6, 1.8, and 3.6 ppm with flow rates of 100 and 300 ml/min. The exposure durations in the Morris (1996) and Struve et al. (2008) studies were 40 and 80 min, respectively. Nasal uptake of acrolein did not attain a steady state in either study. Therefore, for data compatability, the first 40 min of uptake data from Struve et al. (2008) were used to compute a time average for the exposure duration.

The mean body weight of the rats used by Struve et al. (2008) was 196 g and the range of body weights of rats used by Morris (1996) was 170–230 g, while the PK model simulated the rat nose on which the CFD model was based (a 315-g F344 rat). Since the body weights of these rats are different, the flow rates used in the models were allometrically scaled using the following formula for minute volumes at resting breathing (U.S. EPA, 1994):

$$\ln(\mathrm{MV}) = -0.578 + 0.821\ \ln(\mathrm{BW})$$

where MV is minute volume (L/min) and BW is body weight (kg). Using this formula, minute volumes for a 196- and a 315-g rat were estimated to be 147 and 217 ml/min, respectively. Using the scaling that 100 ml/min is 68% of MV and 300 ml/min is 204% of MV for a 196-g rat, corresponding inhalation flow rates for a 315-g rat were 148 and 443 ml/min, respectively.

The PK model uses a simple compartmental description of the rat nose with an epithelial structure similar to the structure implemented in the CFD model. This approach provides a useful method for initially estimating kinetic parameters that can be applied to the nonlinear boundary condition of the CFD model. However, the simplified model structure is most likely not adequate to accurately predict acrolein dynamics in the nose. Nasal extraction of acrolein was shown to be moderate to high, meaning that a large anterior-to-posterior concentration gradient exists throughout the nose. Therefore, the parameters obtained from a simple one-compartment description of the rat nose cannot be expected to provide similar extraction scenarios when used in a CFD model, which predicts the distribution of acrolein dosimetry throughout the nose. Therefore, kinetic parameters initially estimated with the PK model were individually adjusted in the CFD model to improve fits to the NE data. Airflow simulations in the CFD model were also run at 148 and 443 ml/min to be allometrically similar to flow rates used in the experimental nasal uptake studies.

To predict acrolein nasal extraction in human nasal passages, kinetic parameters describing tissue clearance processes in the rat nose were scaled to account for different metabolic rates between rats and humans. A scaling factor based on the surface area of mucus-coated epithelium in the rat and human nasal passages was applied to the first-order clearance term, $k_f V_t$, where V_t is the tissue volume of respiratory and olfactory epithelium, and the maximal metabolic rate, $V_{\max}$. The Michaelis–Menten parameter K_m and the air–tissue partition coefficients were assumed to be species invariant.

Lesion Distribution

The acrolein exposure system and histopathology analysis are described in detail elsewhere (Dorman et al., 2008). Briefly, adult male F344 rats were exposed by inhalation to 0, 0.02, 0.06, 0.2, 0.6, or 1.8 ppm acrolein for 6 h/day, 5 days/wk, for up to 65 exposure days (12 rats/concentration). Nasal histopathology was evaluated after 4, 14, 30, and 65 exposure days, and 60 days after the end of the 65-day exposure period. Transverse nasal sections (5 μm), prepared at six standard levels (Morgan, 1991), were routinely processed, stained with hemotoxylin and eosin, and histologically examined by microscopy. The cross-sectional levels consisted of the nasal tip through squamous epithelium, levels I–IV passing through respiratory/transitional and olfactory epithelium, and level V passing through the nasopharyngeal duct. Nasal histopathology from levels I–IV after 65 exposure days were used in the analysis in this study (Figure 2A).

Cross-sectional airway perimeters from levels I–IV were divided into regions based on anatomical and airflow-associated landmarks (Figure 2B). Regions were numbered consecutively beginning on the ventral aspect of the septum. Regions were of approximately similar length, with the exception of regions 7, 9, 11, and 13 at level IV, which correspond to turbinate structures that receive low fractions of overall airflow (and hence low gas uptake). Respiratory epithelium comprised all of level I and

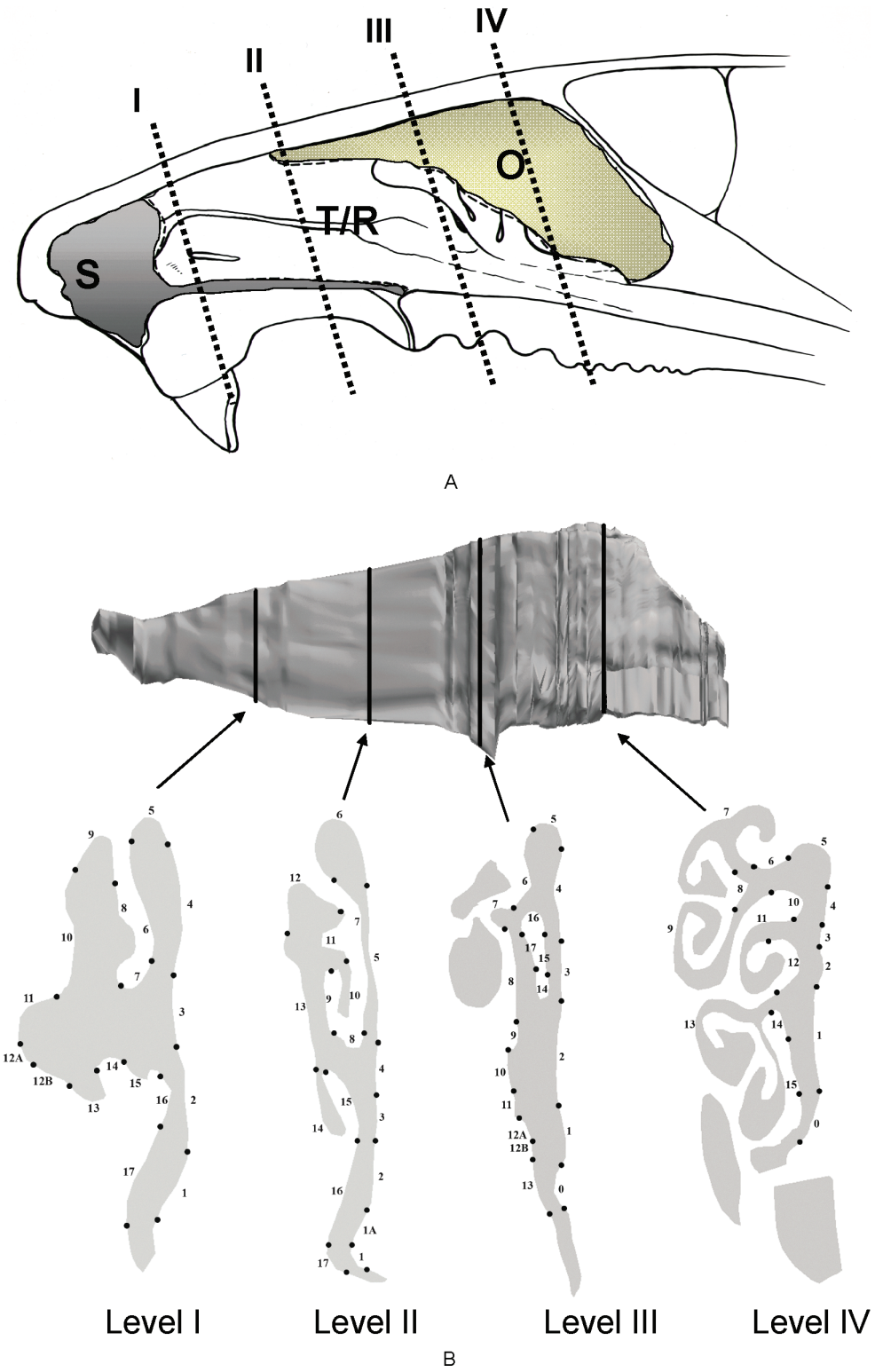

FIG. 2. (A) Schematic of the rat nasal cavity (sagittal view with the septum removed) showing the approximate location of transverse sections (levels I–IV) used for histological examination in Dorman et al. (2008): squamous epithelium (S), transitional/respiratory epithelium (T/R), and olfactory epithelium (O). (B) Septal view of the rat nasal CFD model showing the location of transverse sections where air:tissue flux predictions were made. These locations correspond to those used for histopathological evaluation (A). The perimeters of levels I–IV were divided into small subregions that were used to compare lesion incidence and flux predictions.

most of levels II and III. Olfactory epithelium was present in region 6 (the tip of the dorsal meatus) of level II, regions 4–6 (dorsal meatus) and 16 (dorsal portion of the ethmoturbinate) of level III, and most of level IV (regions 1–15). The presence or absence of respiratory or olfactory lesions in all animals was determined in each region of each level. At each level, epithelium was compared to that occurring in control animals (0 ppm exposure) at the same time point. Lesion incidence (out of 12) was calculated for each region in all four levels.

Flux Predictions

Coronal cross sections corresponding to levels I–IV were identified in the rat nasal CFD model (Figure 2B). Section perimeters were divided into regions identical to those used for lesion incidence mapping. Average air:tissue flux of inhaled acrolein was computed for each region at each level with the rat nasal CFD model. Average flux and lesion incidence in each region at each level were ranked, and a Spearman rank correlation coefficient was determined to test the strength of the correlation between the two sets of data.

RESULTS

Acrolein Nasal Extraction Predictions

The best fit of the PK model to the NE data of Morris (1996) and Struve et al. (2008) was obtained with the parameter values of $k_f = 0.1\ \text{s}^{-1}$, $V_{\max} = 6.0 \times 10^{-3}\ \mu$g/s, and $K_m = 1.0 \times 10^{-3}\ \mu$g/ml (Figure 3) using optimization routines in Matlab (Mathworks, Inc., Natick, MA). NE predicted by the PK model was computed at flow rates of 148 and 443 ml/min for a 315-g rat, corresponding to allometrically equivalent flow rates of 100 and 300 ml/min for a 196-g rat, the mean body weight used in the study by Struve et al. (2008). Although there was a slight overprediction in NE at the lower flow rate, the better fit at the higher flow rate was preferred since this flow rate was close to a flow rate of 434 ml/min, equivalent to resting breathing in a rat.

When the optimized parameters from the PK model were implemented in the nonlinear boundary condition of the CFD model, a general underprediction of the in vivo NE data was observed (Figure 3). To further optimize the parameters for the CFD model, each parameter was individually adjusted until better fits with the NE data were observed, stressing the uptake behavior at the higher physiologic flow rate. Better fits were obtained by slightly decreasing k_f, increasing $V_{\max}$, and decreasing K_m (Table 2). At the lower flow rate, a slight overprediction of the NE data was observed at exposure concentrations >0.6 ppm; at the higher flow rate, excellent agreement was observed between the CFD predictions and the NE data (Figure 4). A significant underprediction of NE was observed at 0.6 ppm at the higher flow rate (61% NE predicted by the CFD model versus 90% NE from Struve et al. (2008)). However, there was a wide range of uptake at the lower concentrations in the experimental studies, ranging from 50% at 0.9 ppm to 90% at 0.6 ppm. This difference in experimental NE values could be partially attributable

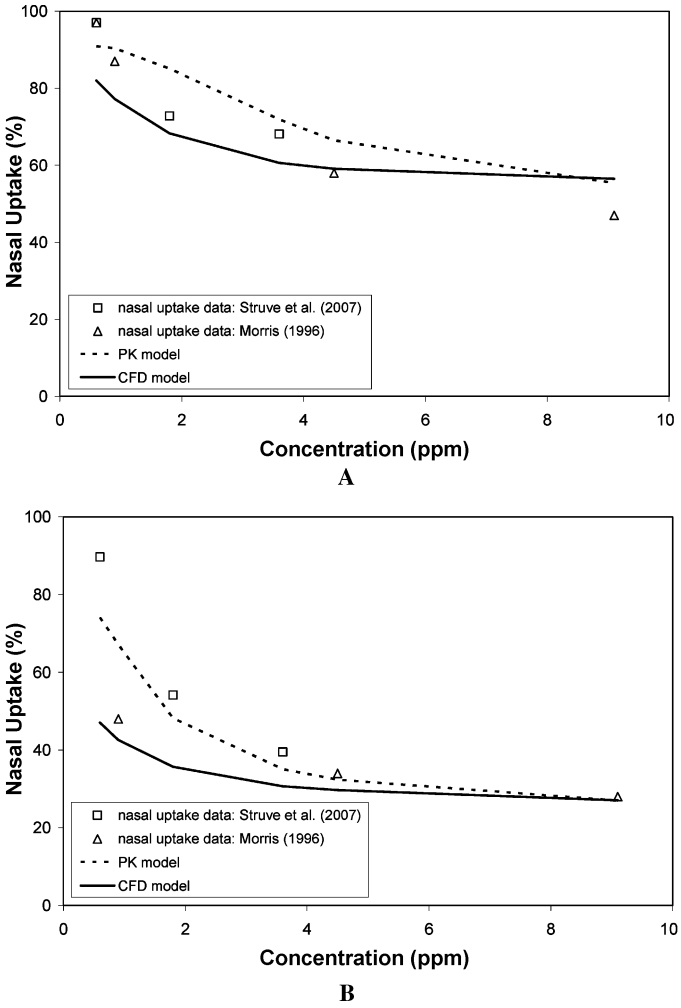

FIG. 3. Comparison of NE predictions from the PK and CFD models with time-averaged NE data. Kinetic parameters used in the PK and CFD models were estimated with the PK model. Flow rates used in the model predictions were allometrically similar to the flow rates used in the experimental uptake study. (A) 100 ml/min (148 ml/min for PK and CFD models); (B) 300 ml/min (443 ml/min for PK and CFD models).

to different inspiratory air temperatures and relative humidities used in the two studies, which, respectively, ranged from 21.7 to 23.0°C and from 45 to 55% in the Struve et al. (2008) study, versus 40°C and 90% in the Morris (1996) study. Despite these

TABLE 2
Estimated kinetic parameters used in the rat and human nasal CFD models

Parameter	Rat	Human
k_f (sec^{-1})	0.05	0.02
$V_{\max}$ (μg/sec)	1.1×10^{-2}	1.375×10^{-1}
K_m (μg/ml)	5.0×10^{-4}	5.0×10^{-4}

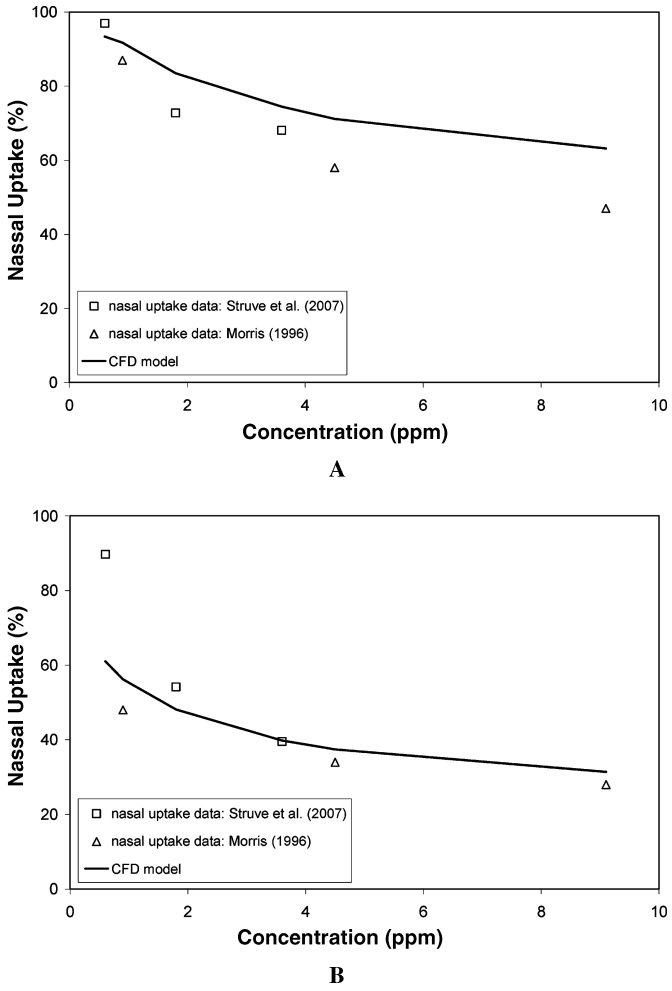

FIG. 4. Comparison of NE predictions from the CFD model with time-averaged NE data. Kinetic parameters were estimated with the CFD model. (A) 100 ml/min (148 ml/min for the CFD model); (B) 300 ml/min (443 ml/min for the CFD model).

discrepancies in NE measured in vivo, the model predictions capture the overall trend of sharply increased uptake with decreased exposure concentration below 4 ppm.

Predicted rat and human NE of inhaled acrolein under resting breathing conditions was evaluated with the corresponding nasal CFD models. Steady-state inspiratory flow rates at twice the estimated minute volume were used: 434 ml/min and 13.8 L/min for the rat and human, respectively (U.S. EPA, 1994) (Figure 5). Human acrolein dosimetry calculations used the kinetic parameters scaled by total respiratory + olfactory surface area (Table 1), resulting in a scaling factor of 12.5 (Table 2). Calculated human acrolein NE was consistently less than that predicted in the rat over a wide range of exposure concentrations, and also demonstrated saturable uptake behavior. Human NE was predicted to be 16% at 3.6 ppm, increasing dramatically as exposure concentrations decreased below 1 ppm. At an exposure concentration of 0.6 ppm, large gradients in wall mass flux were observed

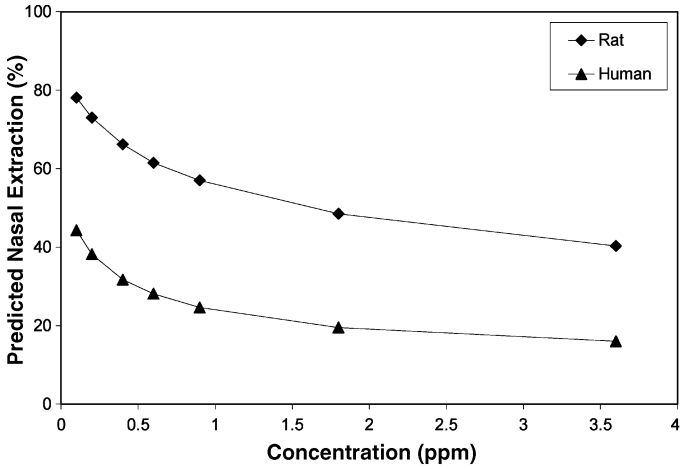

FIG. 5. Comparison of predicted NE from the rat and human nasal CFD models at resting breathing rates: 434 ml/min for the rat, 13.8 L/min for the human.

in the rat on mucus-coated epithelium (Figure 6), as would be expected with the high uptake (∼62%) at this exposure concentration. A more uniform flux distribution was observed in the human nose at this exposure concentration due to the lower uptake (∼28%).

Sensitivity Analysis

A sensitivity analysis was conducted to assess the sensitivity of dosimetry calculations with the rat and human nasal CFD models to the estimated kinetic parameters, air:tissue partition coefficient, nasal blood flow rate, nasal tissue depth, and the squamous mass transfer coefficient (Table 3). The sensitivity of overall nasal extraction and the average flux in the olfactory region were analyzed by computing the resulting average percent change as a result of a ± 50% change in the aforementioned parameters. In addition, the sensitivity of the maximum flux in the olfactory region of the human model was determined, since this value was used in the risk assessment calculations described later in this article. Acrolein nasal dosimetry was found to be insensitive to changes in the first-order rate constant (k_f), the Michaelis–Menten parameter K_m, nasal blood flow, and the squamous mass transfer coefficient; results were mildly sensitive (<22% change) to changes in the maximal metabolic rate ($V_{\max}$), the air:tissue partition coefficient, and total nasal tissue depth.

Correlation of Flux Predictions With Lesion Distribution

Nasal lesions in respiratory epithelium were observed in levels I and II following exposure to 0.6 or 1.8 ppm acrolein. Respiratory lesions in level III were only observed in the 1.8-ppm acrolein dose group. Lesions were observed on olfactory epithelium in levels II–IV following exposure to 1.8 ppm acrolein. No olfactory lesions were observed at exposure concentrations ≤0.6 ppm. A complete description of all types of

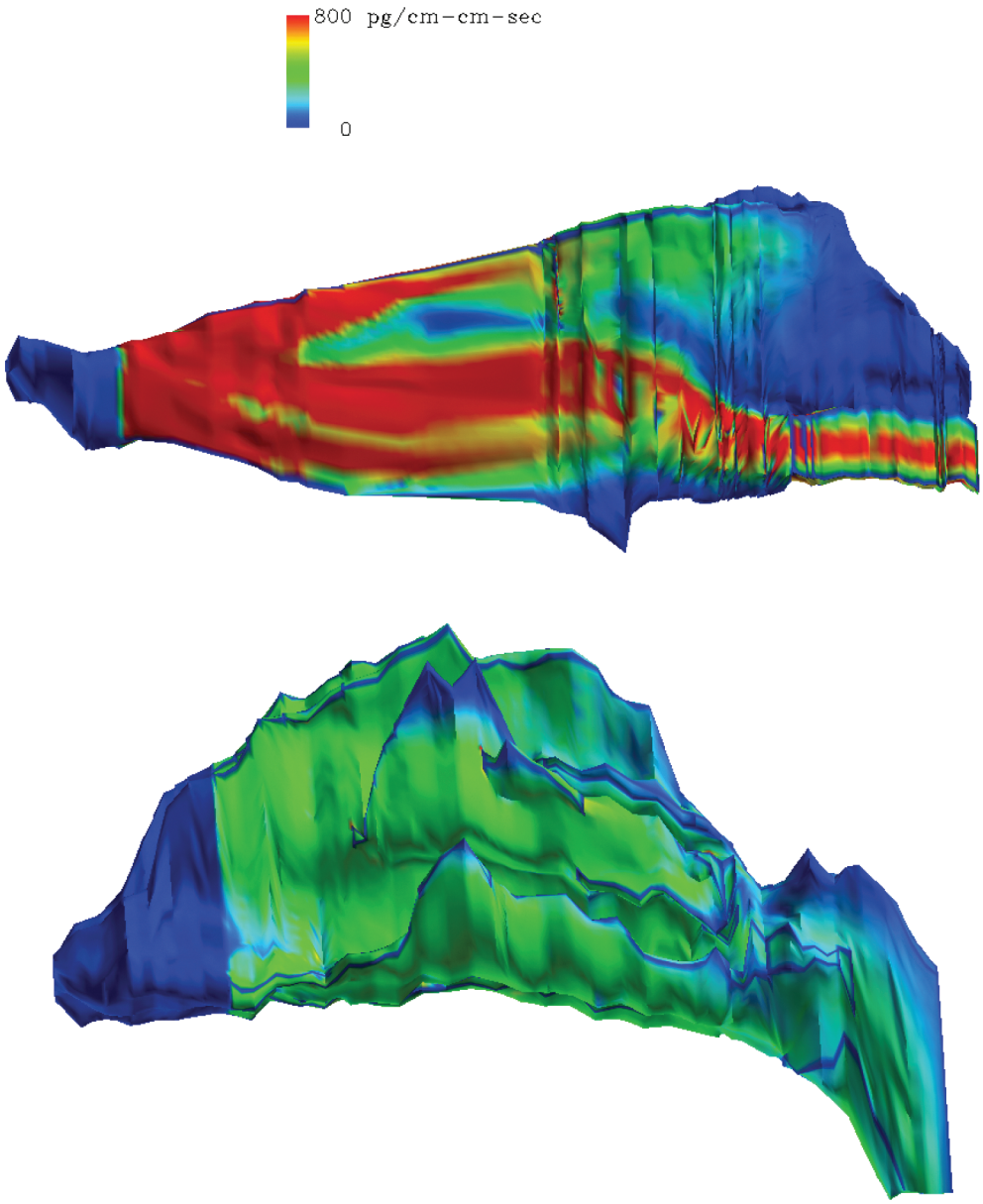

FIG. 6. Wall mass flux of inhaled acrolein in the rat and human nasal passages at steady-state inspiratory airflow rates of 434 ml/min and 13.8 L/min, respectively, at an exposure concentration of 0.6 ppm.

acrolein-induced nasal lesions from a subchronic inhalation study is given in detail elsewhere (Dorman et al., 2008).

Acrolein air:tissue flux predictions showed a gradual decrease in magnitude from levels I–IV. In level I, flux was fairly uniform around the airway perimeters and ranged from 1292 to 2079 pg/cm^2-s at a 1.8-ppm exposure concentration, and from 691 to 1045 pg/cm^2-s at a 0.6-ppm exposure concentration (Table 4). The relatively high uptake efficiency, especially at lower concentrations, leads to high absorption in the anterior regions of the nose. Decreased air:tissue flux levels are found in more distal regions of the nose, where localized flux gradients become more pronounced, with notably high flux along the main airflow streams and low flux in the turbinate regions (Tables 5–7).

In levels I and II, a correlation between predicted air:tissue flux and lesion incidence could not be established due to the high lesion incidence (at or near 100%) in most regions (Tables 4 and 5). In level III, a strong statistical correlation was found between predicted flux and respiratory lesion incidence at an exposure concentration of 1.8 ppm (Table 6, Figure 7A). The rank correlation coefficient was .87 with a p value of .00001. Olfactory lesion incidence (100% in regions 4–6 and 16) was not included in the calculation at level III since the section was primarily comprised of respiratory epithelium. In level IV, a

TABLE 3
Sensitivity analysis for the rat and human nasal CFD models. Individual sensitivity values are an average percent change resulting from a ± 50% change in the independent variable.

	Rat		Human		
Parameter	Nasal Extraction	Average Olfactory Flux	Nasal Extraction	Average Olfactory Flux	Maximum Olfactory Flux
Estimated kinetic parameters:					
k_f	0.3%	0.2%	0.2%	0.2%	0.1%
V_{max}	10.9%	21.9%	17.5%	16.6%	14.7%
K_m	0.5%	0.2%	0.6%	0.5%	0.6%
Partition coefficient ($P_{t:a}$)	13.2%	17.6%	20.2%	19.1%	17.1%
Nasal blood flow (Q_b)	0.3%	0.3%	< 0.1%	< 0.1%	< 0.1%
Squamous mass transfer coefficient (K_s)	0.2%	1.1%	< 0.1%	< 0.1%	< 0.1%
Total nasal tissue depth (L_t+L_b)	12.6%	19.3%	20.0%	18.3%	20.4%

strong correlation was found between predicted flux and olfactory lesion incidence at an exposure concentration of 1.8 ppm, with a rank correlation coefficient of .72 and a p value of .001 (Table 7, Figure 7B).

DISCUSSION

Acrolein nasal extraction in rats was moderate at high concentrations and increased with decreased exposure concentration, indicating saturable metabolism or dose-dependent changes in

TABLE 4
Lesion incidence and predicted air:tissue flux for level I: Respiratory epithelium, regions 1–17

	Lesion incidence (%)[a]		Predicted flux (pg/cm^2-s)	
Region	0.6 ppm	1.8 ppm	0.6 ppm	1.8 ppm
1	0	0	941.1	1821.3
2	0	100	791.9	1629.4
3	0	100	958.3	1852.4
4	100	100	960.4	1834.8
5	100	100	863.4	1730.9
6	100	100	904.8	1718.2
7	83	100	691.0	1291.9
8	50	100	998.7	1890.8
9	0	100	916.5	1938.1
10	0	100	989.2	1862.4
11	0	100	836.7	1598.8
12A	0	100	996.7	1926.2
12B	0	0	1045.3	2079.4
13	0	0	742.5	1582.3
14	0	100	994.0	1935.5
15	0	100	820.1	1660.3
16	0	100	705.9	1472.4
17	0	0	885.6	1702.8

[a] $n = 12$ animals.

TABLE 5
Lesion incidence and predicted air:tissue flux for level II: Respiratory epithelium, regions 1–5, 7–17; olfactory epithelium, region 6

	Lesion incidence (%)[a]		Predicted flux (pg/cm^2-s)	
Region	0.6 ppm	1.8 ppm	0.6 ppm	1.8 ppm
1A	0	33	659.0	1532.3
1B	0	100	182.7	447.2
2	0	100	705.2	1505.9
3	0	100	825.8	1655.5
4	0	100	944.6	1818.5
5	0	92	400.3	1080.8
6	0	100	681.9	1509.1
7	0	100	362.8	1034.6
8	0	100	782.8	1502.4
9	0	100	928.1	1845.9
10	0	100	81.1	367.3
11	0	100	729.1	1425.8
12	0	100	829.7	1755.0
13	100	100	974.8	1921.2
14	0	100	146.7	705.1
15	0	100	981.3	2018.9
16	0	100	696.2	1497.6
17	0	0	482.4	1120.1

[a] $n = 12$ animals.

TABLE 6
Lesion incidence and predicted air:tissue flux for level III at 1.8 ppm exposure concentration, with no lesions reported at 0.6 ppm exposure concentration: Respiratory epithelium, regions 0–3, 7–15, 17; olfactory epithelium, regions 4–6, 16

	Lesion incidence (%)[a]	Predicted flux (pg/cm^2-s)	
Region	1.8 ppm	0.6 ppm	1.8 ppm
0	0	278.3	909.8
1	58	534.5	1268.0
2	83	692.9	1437.9
3	50	268.3	849.5
4	100	402.2	1052.2
5	100	436.4	1146.1
6	100	444.2	1162.8
7	8	331.7	1107.8
8	25	376.2	1046.4
9	75	883.1	1988.9
10	58	735.2	1671.2
11	83	761.9	1672.4
12A	92	764.3	1759.5
12B	67	482.1	1248.4
13	0	232.0	708.9
14	33	466.3	1306.7
15	0	240.0	815.5
16	100	331.3	933.2
17	0	222.7	768.6

[a] $n = 12$ animals.

TABLE 7
Lesion incidence and predicted air:tissue flux for level IV at 1.8 ppm exposure concentration, with no lesions reported at 0.6 ppm exposure concentration: Olfactory epithelium, regions 1–15

	Lesion incidence (%)[a]	Predicted flux (pg/cm^2-s)	
Region	1.8 ppm	0.6 ppm	1.8 ppm
1	33	76.4	531.5
2	83	132.1	667.7
3	100	145.5	641.1
4	92	191.2	797.4
5	100	120.5	651.5
6	83	75.4	425.7
7	17	0.8	9.1
8	67	9.7	109.1
9	10[b]	1.5	13.1
10	100	138.6	647.2
11	58	8.6	71.6
12	83	104.6	568.3
13	0	1.3	18.9
14	25	73.9	596.9
15	0	68.0	543.2

[a] $n = 12$ animals.
[b] $n = 10$ animals; 2 animals were determined not to have olfactory epithelium in this region.

reactive processes in nasal tissue. The physiological CFD models developed in this study incorporated air- and tissue-phase diffusivity, solubility, blood flow, and first-order and saturable clearance pathways in a multilayered epithelial structure to account for mass transfer of acrolein from the air phase. The model successfully predicted acrolein nasal extraction over a wide range of exposure concentrations when compared with time-averaged nasal uptake data.

In addition to measuring nasal uptake of inhaled acrolein in naive rats, Struve et al. (2008) also measured nasal uptake in rats that had been preexposed to acrolein. Specifically, nasal uptake of inhaled acrolein at exposure concentrations of 1.8 or 3.6 ppm was measured at a constant unidirectional flow rate of 100 ml/min for 80 min in animals that were preexposed to either 0.6 or 1.8 ppm acrolein for 14 exposure days. Nasal uptake in the preexposed animals was also dependent on exposure concentration and duration. The preexposed animals exhibited higher nasal uptake than the naive animals over the course of the exposure duration. Overall mean nasal uptake efficiency in preexposed animals was approximately 13 to 38% higher than in air-exposed controls. Although preexposure did affect overall nasal uptake, these measurements were not used in this study. The uptake data consisting of naive animals exposed to acrolein at multiple flow rates over a wide range of exposure concentrations provided by Morris (1996) and Struve et al. (2008) provided a richer data set to compare model predictions. Acrolein exposure has been shown to induce nasal vasodilation, increase nasal blood flow, and progressively thicken the air:blood barrier, possibly altering inhalation airflow patterns (Morris, 1996; Morris et al., 1999; Struve et al., 2008). These potential effects were not taken into account with the CFD models. However, dosimetry calculations were shown to be insensitive to nasal blood flow rate and mildly sensitive to nasal tissue depth.

Regional flux predictions from the rat nasal CFD model correlated well with acrolein-induced lesion incidence from a subchronic inhalation study (Dorman et al., 2008). There were also individual regions, most notably in levels I and II, that were predicted to receive high tissue dose but did not see as severe a response as other regions with lower tissue doses. These discrepancies could be attributed to numerical errors with flux predictions on irregularly shaped boundaries or sensitivity of response data to region demarcations, but could also potentially indicate different levels of localized sensitivity among epithelial types.

Flux predictions indicate that the olfactory epithelium in level IV generally received a lower tissue dose than the more anterior

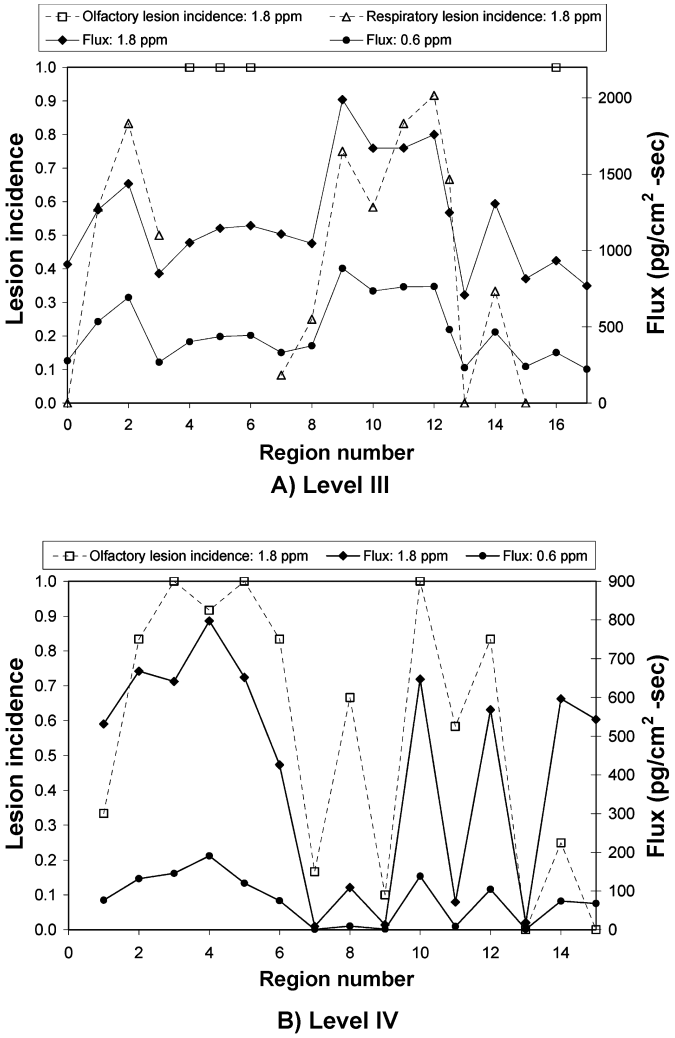

FIG. 7. Acrolein-induced respiratory and olfactory lesion incidence compared with predicted acrolein air:tissue flux at exposure concentrations of 0.6 and 1.8 ppm. No lesions were observed following 0.6 ppm exposure. (A) Level III; (B) level IV.

respiratory epithelium where lesions were also present at an exposure concentration of 1.8 ppm, and also received a lower tissue dose than the olfactory epithelium on the dorsal meatus in levels II and III that borders the main dorsal airflow stream. These observations suggest that acrolein lesion incidence is related not only to tissue dose, but also to tissue type, and that the olfactory epithelium is more sensitive than respiratory epithelium to inhaled acrolein. Flux predictions from the anterior regions of the nose in levels I and II were consistently higher than those in levels III and IV, and lesions at these levels were reported near 100% incidence. Acrolein is a highly soluble and reactive gas, which should lead to rapid uptake in the anterior mucus-coated regions of the nose, and a concentration gradient progressing distally through the nose, leading to lower concentrations and lower tissue dose in the more posterior regions.

The current inhalation RfC for acrolein is 2×10^{-5} mg/m^3 ($\sim$0.009 ppb) (Integrated Risk Information System, http://www.epa.gov/iris, accessed May 2007), based on nasal pathology in rats with a lowest-observed-adverse-effect level (LOAEL) of 0.4 ppm (Feron et al., 1978). The RfC is an estimate of a continuous inhalation exposure to humans that is likely to be without appreciable risk of adverse effects over a person's lifetime (U.S. EPA, 1994). A minimal LOAEL was used in the absence of a NOAEL for nasal pathology.

Recently, Dorman et al. (2008) further characterized the nasal toxicity of acrolein using lower exposure concentrations than those in previous studies to establish a NOAEL. They identified NOAELs of 0.2 ppm for respiratory epithelial responses and 0.6 ppm for olfactory neuronal loss. Respiratory epithelial responses included respiratory epithelial hyperplasia, inflammation, and squamous metaplasia of the respiratory epithelium. The most severely affected site occurred along the lateral wall of level II. Although this lesion occurred at a lower exposure concentration than the olfactory epithelial response, the rostral–caudal gradient in tissue doses observed in the present study demonstrated that olfactory epithelial responses occurred at lower tissue dose. This observation helped to justify our use of the olfactory lesions as the critical effect in deriving a tissue-dose based NOAEL and applying this value to determine human health risks associated with inhaled acrolein.

Standard inhalation RfC calculations by the U.S. EPA for soluble, reactive gases rely on dosimetric adjustment factors that are used to account for species differences in delivered dose to convert a NOAEL to a NOAEL$_{[\mathrm{HEC}]}$ (U.S. EPA, 1994). Once a NOAEL is identified, an adjusted NOAEL, NOAEL$_{[ADJ]}$, is computed to convert to continuous exposure conditions (6 to 24 h/day, 5 to 7 days/wk in this case). This value is then multiplied by the regional gas dose ratio (RGDR) to obtain the NOAEL$_{[\mathrm{HEC}]}$. The RGDR is the relative minute-volume-to-upper-respiratory-tract-surface-area ratio between the rat and human and assumes complete extraction of the gas with a uniform dose throughout the respiratory tract.

Although dosimetric adjustment factors consider differences in respiration and gross upper respiratory tract anatomy between species, they do not account for interspecies differences in localized airflow patterns, concentration gradients, or clearance processes. Clearly, the two assumptions used in the RGDR calculations are not valid when considering nasal dose of inhaled acrolein (i.e., nasal uptake is $<$100% and is nonuniformly distributed throughout the nose). Physiological CFD models of the rat and human nasal passages help quantify these interspecies differences in airflow and uptake patterns to refine human risk estimates based on nasal effects. The CFD models used in this study were used to overcome the limitations of the simplifying interspecies adjustment factors by using flux predictions as a tissue-dose surrogate to derive a tissue-dose-based NOAEL (i.e., the highest predicted tissue dose where lesions were not observed), which can then be translated to a tissue-dose-based NOAEL$_{[\mathrm{HEC}]}$ based on equivalent flux predictions

between species. Use of nasal CFD models should also result in a reduction in the uncertainty for interspecies extrapolation of inhaled dose.

Acrolein flux predictions were calculated using the rat nasal CFD model at the NOAEL (0.6 ppm) and LOAEL (1.8 ppm) for olfactory neuronal loss from the Dorman et al. (2007) study. In level IV, comprised entirely of olfactory epithelium, the highest predicted flux at the NOAEL occurred in region 4, and was 191 pg/cm^2-s. Relatively high flux values (74–191 pg/cm^2-s) were also observed in regions 1–6, 8, 10, 12, and 14–15. Based on these predictions, a tissue-dose-based NOAEL was 191 pg/cm^2-s. However, lesions in fact were observed at an exposure concentration of 1.8 ppm where flux values <191 pg/cm^2-s were predicted with the CFD model. The lowest flux values were observed in regions 7, 9, and 13. However, no lesions were reported in 13, and the number of lesions reported in regions 7 and 9 (2/12 and 1/10, respectively), did not represent a statistically significant increase over control animals (Dorman et al., 2007). In regions 8 and 11, relatively low flux values, 109 and 72 pg/cm^2-s, respectively, were observed with moderately high lesion incidence (8/12 and 7/12, respectively). Region 8 corresponds to the mid-medial aspect of the second ethmoturbinate; region 11 comprises the ventral margin of the dorsal scroll of the third ethmoturbinate and the lateral and dorso-lateral aspects of the ventral scroll of the third ethmoturbinate (using the terminology in Mery et al., 1994) (Figure 8). The lesser of these values, 72 pg/cm^2-s in region 11, was considered a threshold flux value for olfactory lesions in the rat nose. Flux predictions in region 11 of level IV were associated with mild cellular disorganization and epithelial injury. Other sites with higher fluxes, including the dorsal meatus, were associated with more severe injury including olfactory neuronal loss (Dorman et al., 2008). This approach of selecting the region with the lowest flux value associated with less extensive injury should result in a conservative estimate of the local tissue dose needed to induce an adverse response. This flux value can therefore be considered a tissue-dose-based NOAEL since it represents a more conservative approach than using the highest flux value at the NOAEL (Schroeter et al., 2006b).

Assuming that equal tissue doses will invoke similar responses in olfactory epithelium of rats and humans, the threshold flux value derived earlier can be used to estimate an equivalent human exposure concentration that would potentially lead to olfactory lesions in the human nose. Human olfactory flux values were calculated over a wide range of acrolein exposure concentrations (Figure 9A). For each concentration, flux values at each nodal point in the olfactory region were rank-ordered to determine the maximum and 99th percentile values (i.e., the flux value greater than or equal to 99% of flux values in the olfactory region). The 99th percentile values were used in the following risk calculations to overcome possible inaccuracies computing wall mass fluxes over complex geometries such as those found in the nasal passages. We found that an exposure concentration of ~45 ppb induces a 99th percentile olfactory flux value that is equal to the threshold flux value in the rat of 72 pg/cm^2-s

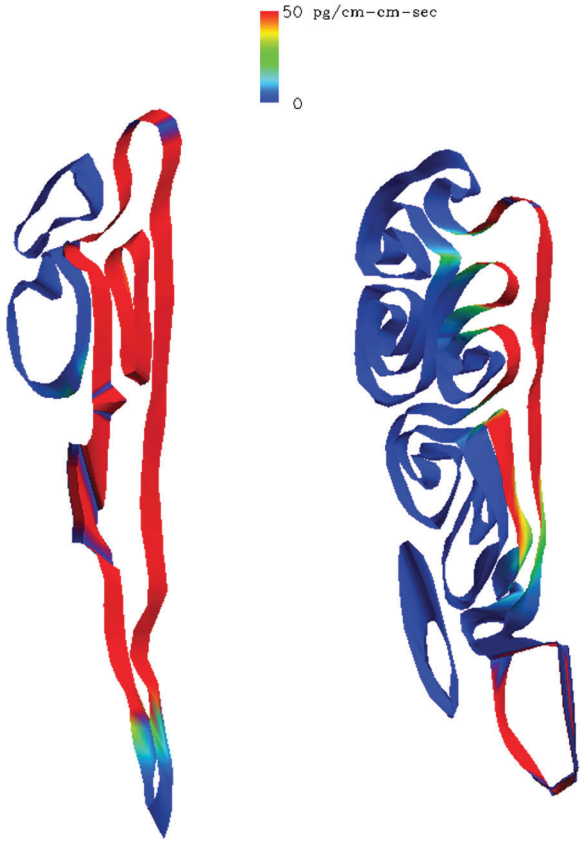

FIG. 8. Flux predictions at levels III and IV in the rat nasal CFD model at an exposure concentration of 0.6 ppm. High flux values were observed along the main ventral and dorsal airflow streams, with lower flux present in the turbinate regions. Moderately high flux was observed in region 8 and the ventral margin of the dorsal scroll of the third ethmoturbinate in region 11 (see Figure 2B for numbered region locations) where moderately high lesion incidence was observed.

(Figure 9A). Following a protocol similar to that of the U.S. EPA in their RfC calculations, this exposure concentration was then adjusted to account for noncontinuous exposure conditions used in the subchronic acrolein inhalation study (i.e., × 6/24 h/day × 5/7 days/wk). Although this time adjustment would typically be applied at the level of target tissue flux, convergence issues with the CFD models at low concentrations (in the low ppb range) led us to apply the adjustment to the human exposure concentration associated with the target tissue flux. The tissue-dose-based NOAEL$_{[HEC]}$ for acrolein was therefore estimated to be ~8 ppb.

To further examine how predicted fluxes were distributed across the human olfactory region at an exposure concentration of 45 ppb, the olfactory surface area was partitioned into bins based on acrolein tissue flux (Figure 9B). An individual flux bin represents the portion of the olfactory surface area that receives flux within a specified range. Olfactory flux values from

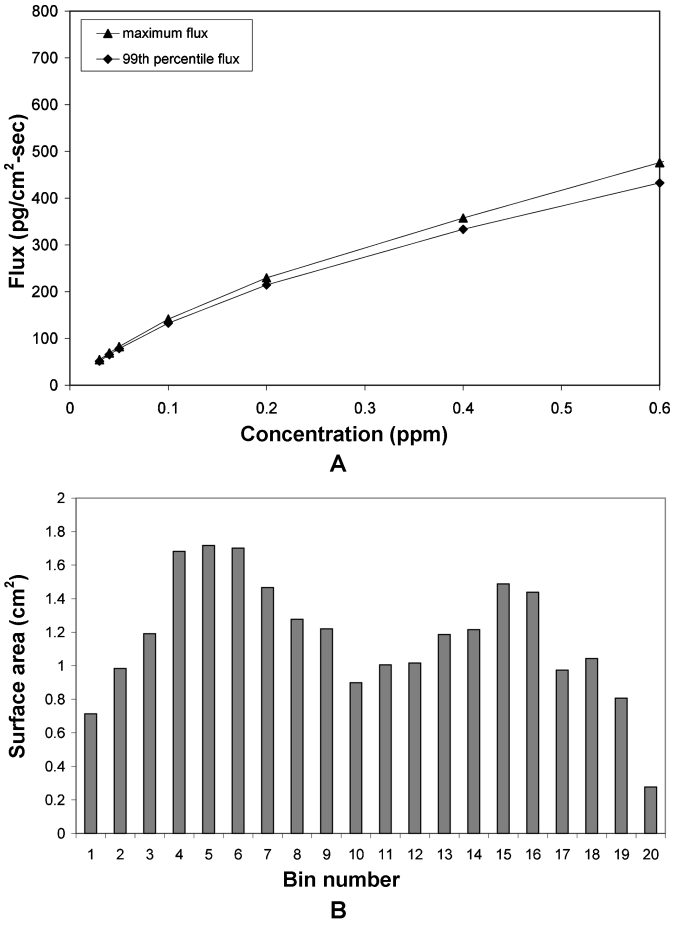

FIG. 9. (A) Maximum and 99th percentile flux values in the human olfactory region predicted by the CFD model for acrolein exposure concentrations ranging from 0.03 to 0.6 ppm. An exposure concentration of 45 ppb was identified to correspond to a 99th percentile threshold flux value of 72 pg/cm^2-s. (B) Human olfactory surface area partitioned by predicted acrolein air:tissue flux at an exposure concentration of 45 ppb. The minimum flux was 0 and the maximum flux was 76 pg/cm^2-s. The 99th percentile flux value of 72 pg/cm^2-s was located in bin 19.

0 to 76 pg/cm^2-s were partitioned into 20 equally spaced bins, with bin 1 containing the surface area associated with the lowest 5% flux values, and bin 20 containing the surface area with the highest 5% flux values. A fairly uniform flux distribution was observed throughout the olfactory region. At this exposure concentration, the 99th percentile flux value resided in bin 19, indicating the use of a conservative value for risk estimates, as opposed to the 95th percentile value (in bin 18), or the average olfactory flux (in bin 10). The highest flux values were observed in the anterior portion of the olfactory epithelium, which is consistent with the pathological findings indicating a rostral–caudal lesion severity gradient with the anterior olfactory region being more severely affected (Dorman et al., 2008).

In RfC calculations, the U.S. EPA generally applies a variety of uncertainty factors (UFs) to the NOAEL$_{[HEC]}$. Uncertainty factors used by the U.S. EPA for acrolein included a UF = 3 for interspecies extrapolation (to account for possible species differences in pharmacodynamics), UF = 10 for human variability, UF = 10 for adjustment from subchronic to chronic duration, and UF = 3 to account for the lack of a NOAEL (i.e., LOAEL to NOAEL conversion).

The scientific merit of using a subchronic-to-chronic factor should be considered. Although the study on which the assessment is based was only of 90 days duration (Dorman et al., 2008) responses seen in this subchronic study encompassed the vast majority of animals (i.e., >90% of the olfactory epithelium was affected), occurred with high incidence rates (>80%), and had reached near maximal severity intensity. Moreover, chronic studies with acrylate esters, another chemical that induces similar responses in the olfactory epithelium, suggest that little to no progression of the olfactory epithelial lesion developed after the end of a subchronic exposure (i.e., lesions seen at 2 yr were similar to those seen following 3 to 12 mo of exposure) (Frederick et al., 1994; Lomax et al., 1997; Miller et al., 1985; Reininghaus et al., 1991). The results from these studies indicate that a UF for subchronic to chronic duration of exposure is unlikely to be needed for agents that primarily target the olfactory neuron.

In summary, anatomically accurate physiological CFD models of the rat and human nasal passages were used to predict interspecies dosimetry of inhaled acrolein. A refined estimate of a NOAEL$_{[HEC]}$ = 8 ppb for acrolein was derived based on quantitative tissue dose predictions rather than default dosimetric assumptions for interspecies extrapolation. The dosimetric approach used in the present study was based on multiple conservative assumptions, deriving a tissue-dose-based NOAEL using site-specific flux predictions at the most sensitive site in the rat nose associated with mild olfactory injury, and basing human predictions on maximal olfactory tissue dose. Interspecies CFD models provide a method to extrapolate effects in laboratory animals to human exposure conditions on the basis of localized tissue dose and response and can be used to reduce uncertainty in risk estimates. Application of a composite uncertainty factor of 30 (for human variability and possible species differences in pharmacodynamics) was applied to this tissue dose-based NOAEL$_{[HEC]}$ of 8 ppb to obtain a proposed inhalation RfC of 0.27 ppb.

REFERENCES

Agency for Toxic Substances and Disease Registry. 1990. Toxicological profile for acrolein. Atlanta, GA: U. S. Public Health Service, TP-90–01.

Andersen, M. E., and Sarangapani, R. 1999. Clearance concepts applied to the metabolism of inhaled vapors in tissues lining the nasal cavity. *Inhal. Toxicol.* 11:873–897.

Beauchamp, R. O., Andjelkovich, D. A., Klingerman, A. D., Morgan, K. T., and Heck, H. d'A. 1985. A critical review of the literature on acrolein toxicity. *Crit. Rev. Toxicol.* 14:309–380.

Bogdanffy, M. S., Sarangapani, R., Plowchalk, D. R., Jarabek, A., and Andersen, M. E. 1999. A biologically based risk assessment for vinyl acetate-induced cancer and noncancer inhalation toxicity. *Toxicol. Sci.* 51:19–35.

Brown, R. P., Delp, M. D., Lindstedt, S. L., Rhomberg, L. R., and Beliles, R. P. 1997. Physiological parameter values for physiologically based pharmacokinetic models. *Toxicol. Ind. Health* 13:407–484.

Brunnemann, K. D., Kagan, M. R., Cox, J. E., and Hoffmann, D. 1990. Analysis of 1,3-butadiene and other selected gas-phase components in cigarette mainstream and sidestream smoke by gas chromatography–mass selective detection. *Carcinogenesis* 11:1863–1868.

Buckley, L. A., Jiang, X. Z., James, R. A., Morgan, K. T., and Barrow, C. S. 1984. Respiratory tract lesions induced by sensory irritants at the RD50 concentration. *Toxicol. Appl. Pharmacol.* 74:417–429.

Cassee, F. R., Groten, J. P., and Feron, V. J. 1996. Changes in the nasal epithelium of rats exposed by inhalation to mixtures of formaldehyde, acetaldehyde, and acrolein. *Fundam. Appl. Toxicol.* 29:208–218.

Dorman, D. C., Struve, M. F., Wong, B. A., Marshall, M. A., Gross, E. A., and Willson, G. 2007. Respiratory epithelial cell responses in male rats following subchronic acrolein inhalation. *Inhal. Toxicol.*

Feron, V. J., Kruysse, A., Til, H. P., and Immel, H. R. 1978. Repeated exposure to acrolein vapor: Subacute studies in hamsters, rats and rabbits. *Toxicology* 9:47–57.

Frederick, C. B., Bush, M. L., Lomax, L. G., Black, K. A., Finch, L., Kimbell, J. S., Morgan, K. T., Subramaniam, R. P., Morris, J. B., and Ultman, J. S. 1998. Application of a hybrid computational fluid dynamics and physiologically based inhalation model for interspecies dosimetry extrapolation of acidic vapors in the upper airways. *Toxicol. Appl. Pharmacol.* 152:211–231.

Frederick, C., Udinsky, J. and Finch, L. 1994. The regional hydrolysis of ethyl acrylate to acrylic acid in the rat nasal cavity. *Toxicol. Lett.* 70:49–56.

Jarabek, A. M., Kimbell, J. S., Schlosser, P. M., Lou, S. R., and Hanna, L. M. 2001. Computational fluid dynamics and mass transport calculations update the inhalation reference concentration methods: Rat. *Toxicol. Sci.* 60:150.

Kimbell, J. S., Godo, M. N., Gross, E. A., Joyner, D. R., Richardson, R. B., and Morgan, K. T. 1997a. Computer simulation of inspiratory airflow in all regions of the F344 rat nasal passages. *Toxicol. Appl. Pharmacol.* 145:388–398.

Kimbell, J. S., Gross, E. A., Richardson, R. B., Conolly, R. B., and Morgan, K. T. 1997b. Correlation of regional formaldehyde flux predictions with the distribution of formaldehyde-induced squamous metaplasia in F344 rat nasal passages. *Mutat. Res.* 380:143–154.

Kimbell, J. S., Overton, J. H., Subramaniam, R. P., Schlosser, P. M., Morgan, K. T., Conolly, R. B., and Miller, F. J. 2001a. Dosimetry modeling of inhaled formaldehyde: Binning nasal flux predictions for quantitative risk assessment. *Toxicol. Sci.* 64:111–121.

Kimbell, J. S., Subramaniam, R. P., Gross, E. A., Schlosser, P. M., and Morgan, K. T. 2001b. Dosimetry modeling of inhaled formaldehyde: Comparisons of local flux predictions in the rat, monkey, and human nasal passages. *Toxicol. Sci.* 64:100–110.

Lam, C. W., Casanova, M., and Heck, H. D. 1985. Depletion of nasal mucosal glutathione by acrolein and enhancement of formaldehyde-induced DNA-protein cross-linking by simultaneous exposure to acrolein. *Arch. Toxicol.* 58:67–71.

Loden, M. 1986. The in vitro permeability of human skin to benzene, ethylene glycol, formaldehyde, and *n*-hexane. *Acta Pharmacol. Toxicol.* 58:382–389.

Lomax, L., Krivanek, N., and Frame, S. 1997. Chronic inhalation toxicity and oncogenicity of methyl methacrylate in rats and hamsters. *Food Chem. Toxicol.* 35: 393–407.

Mery, S., Gross, E. A., Joyner, D. R., Godo, M., and Morgan, K. T. 1994. Nasal diagrams: A tool for recording the distribution of nasal lesions in rats and mice. *Toxicol. Pathol.* 22:353–372.

Miller, R. R., Young, J. T., Kociba, R. J., Keyes, D. G., Bodner, K. M., Calhoun, L. L., and Ayres, J. A. 1985. Chronic toxicity and oncogenicity bioassay of inhaled ethyl acrylate in Fischer 344 rats and B6C3F1 mice. *Drug Chem. Toxicol.* 8:1–42.

Morgan, K. T. 1991. Approaches to the identification and recording of nasal lesions in toxicology studies. *Toxicol. Pathol.* 19:337–351.

Morris, J. B. 1996. Uptake of acrolein in the upper respiratory tract of the F344 rat. *Inhal. Toxicol.* 8:387–403.

Morris, J. B., Hassett, D. N., and Blanchard, K. T. 1993. A physiologically based pharmacokinetic model for nasal uptake and metabolism of nonreactive vapors. *Toxicol. Appl. Pharmacol.* 123:120–129.

Morris, J. B., Stanek, J., and Gianutsos, G. 1999. Sensory nerve-mediated immediate nasal responses to inspired acrolein. *J. Appl. Physiol.* 87:1877–1886.

Plowchalk, D. R., Andersen, M. E., and Bogdanffy, M. S. 1997. Physiologically based modeling of vinyl acetate uptake, metabolism, and intracellular pH changes in the rat nasal cavity. *Toxicol. Appl. Pharmacol.* 142:386–400.

Reininghaus, W., Koestner, A., and Klimisch, H.-J. 1991. Chronic toxicity and oncogenicity of inhaled methyl acrylate and *n*-butyl acrylate in Sprague-Dawley rats. *Food Chem. Toxicol.* 29:329–339.

Roemer, E., Anton, H. J., and Kindt, R. 1993. Cell proliferation in the respiratory tract of the rat after acute inhalation of formaldehyde or acrolein. *J. Appl. Toxicol.* 13:103–107.

Sarangapani, R., Teeguarden, J. G., Gentry, P. R., Clewell, H. J., Barton, H. A., and Bogdanffy, M. S. 2004. Interspecies dose extrapolation for inhaled dimethyl sulfate: A PBPK model-based analysis using nasal cavity N^7-methylguanine adducts. *Inhal. Toxicol.* 16:593–605.

Schroeter, J. D., Kimbell, J. S., Bonner, A. M., Roberts, K. C., Andersen, M. E., and Dorman, D. C. 2006a. Incorporation of tissue reaction kinetics in a computational fluid dynamics model for nasal extraction of inhaled hydrogen sulfide in rats. *Toxicol. Sci.* 90:198–207.

Schroeter, J. D., Kimbell, J. S., Andersen, M. E., and Dorman, D. C. 2006b. Use of a pharmacokinetic-driven computational fluid dynamics model to predict nasal extraction of hydrogen sulfide in rats and humans. *Toxicol. Sci.* 94:359–367.

Slaughter, J. C., Koenig, J. Q., and Reinhardt, T. E. 2004. Association between lung function and exposure to smoke among firefighters at prescribed burns. *J. Occup. Environ. Hyg.* 1:45–49.

Struve, M. F., Wong, V. A., Marshall, M. W., Kimbell, J. S., Schroeter, J. D., and Dorman, D. C. 2007. Nasal uptake of inhaled acrolein in rats. *Inhal. Toxicol.*

Subramaniam, R. P., Richardson, R. B., Morgan, K. T., Guilmette, R. A., and Kimbell, J. S. 1998. Computational fluid dynamics simulations of inspiratory airflow in the human nose and nasopharynx. *Inhal. Toxicol.* 10:91–120.

Treitman, R. D., Gurgess, W. A., and Gold, A. 1980. Air contaminants encountered by fire-fighters. *Am. Ind. Hyg. Assoc. J.* 41:796–803.

U. S. Environmental Protection Agency. 1994. Methods for derivation of inhaled reference concentrations and application of inhalation

dosimetry. Washington, DC: Office of Research and Development. EPA/600/8-90-066F.

APPENDIX A

Transport of inhaled acrolein in the nasal passages is governed by convection with inhaled air and molecular diffusion onto airway walls. Convection (airflow) was simulated in 3D by the Navier–Stokes equations, which in the steady-state form for a viscous incompressible fluid are given by:

$$\rho(u \cdot \nabla u) = -\nabla p + \mu \nabla^2 u \quad [A1]$$

$$\nabla \cdot u = 0 \quad [A2]$$

where the solution variables u and p are the air velocity and pressure, and ρ and μ are the density and viscosity of air, respectively. Equations (A1) and (A2) are the momentum and continuity equations, respectively.

At low concentrations, the presence of gas does not affect airflow behavior, so the air-phase transport of acrolein was solved decoupled from Eq.s (A1)–(A2). The convection-diffusion equation is:

$$u \cdot \nabla C = D_a \nabla^2 C \quad [A3]$$

where u is the air velocity from (A1)–(A2), C is the concentration of inhaled acrolein, and D_a is the diffusivity of acrolein in air.

The mucus-coated epithelial structure lining the air phase of the CFD model consisted of a lumped mucus/tissue layer and a submucosal layer (Figure A1). In each of these layers, one-dimensional diffusion and first-order and saturable metabolic processes were simulated with the reaction-diffusion equation. In addition, in the submucosal layer, acrolein was cleared by blood perfusion. Mass transfer in the epithelial layer was governed by the steady-state reaction-diffusion equation:

$$D_t \frac{d^2 C_t}{dx^2} = k_f C_t + \frac{(V_{\max}/V_t) \cdot C_t}{K_m + C_t} \quad [A4]$$

where D_t is the diffusivity of acrolein in tissue, V_t is the volume of the epithelial layer, and C_t is the acrolein concentration in the epithelial layer. Mass transfer in the submucosal layer was governed by the steady-state reaction diffusion equation with the addition of a sink term to account for loss of acrolein to effluent venous blood:

$$D_b \frac{d^2 C_b}{dx^2} = k_f C_b + \frac{(V_{\max}/V_b) \cdot C_b}{K_m + C_b} + (Q_b/V_b) \cdot C_b \quad [A5]$$

where D_b is the diffusivity of acrolein in blood, V_b is the volume of the submucosal layer, Q_b is the blood flow rate, and C_b is the acrolein concentration in the submucosal layer. The diffusivity of acrolein in tissue and blood was set to the diffusivity of acrolein in water.

Using the equilibrium condition across each boundary interface, Equations A4 and A5 are subject to the following boundary conditions:

$C = P_{t:a} C_{air}$ on the tissue side of the air:tissue interface.
$C = P_{b:t} C_{ti}$ on the blood side of the tissue:blood interface.
$C = 0$ at the edge of the submucosal layer.

The $C = 0$ boundary condition implies that any remaining acrolein present in the submucosal layer is rapidly cleared by blood perfusion.

The solutions to the one-dimensional equations (A4)–(A5) were coupled with the 3D convection-diffusion equation (A3) to solve for the air:tissue flux in the normal direction at every boundary nodal point corresponding to nonsquamous epithelium in the computational mesh. Diffusion and reaction in the longitudinal reaction were assumed to be negligible and were not included in this model. While an analytical solution exists to the one-dimensional reaction-diffusion equation with first-order kinetics, the presence of the nonlinear term with Michaelis–Menten kinetics means an analytical solution is not available. Therefore, Eqs. (A4)–(A5) were solved numerically with a Newton-based implicit central finite difference scheme. The concentration gradient through the nasal tissue layers is thereby a function of the local air phase concentration, kinetic parameters, blood flow, and tissue depths. The concentration gradient near the air:tissue boundary determines the rate of absorption (flux) from the air phase into nasal tissue, as given by the following equation for diffusive flux continuity:

$$D_a \left.\frac{\partial C}{\partial n}\right|_{wall}^{air} = D_t \left.\frac{dC}{dx}\right|_{x=0}^{tissue} \quad [A6]$$

where n is the outward normal vector at the boundary of the CFD model, and x is along the direction of the normal vector. Equation

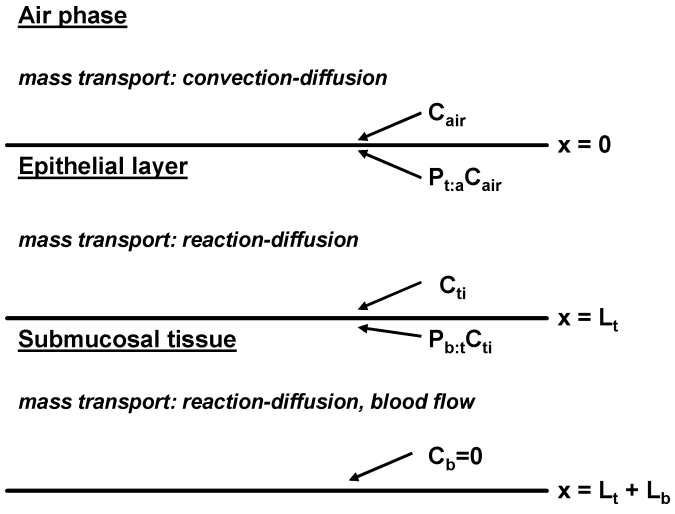

FIG. A1. Schematic of mass transfer in the mucus-coated epithelial structure of the rat and human nasal CFD models. C_{air}, concentration in the boundary layer of the air phase; x, depth from the air:tissue interface into tissue; $P_{t:a}$, tissue:air partition coefficient; $P_{b:t}$, blood:tissue partition coefficient; C_{ti}, concentration on the tissue side of the tissue:blood interface; L_t, depth of the epithelial layer; L_b, depth of the submucosal layer.

(A6) was coupled with the flux boundary condition [Eq. (1) in the text] to numerically compute the air-phase mass transfer coefficient at every boundary nodal point in the computational mesh.

APPENDIX B

A pharmacokinetic model of the rat nose was developed consisting of well-mixed compartments for the air phases of the nasal vestibule and the remaining airway lumen lined by nonsquamous epithelium. A multilayered compartmental structure consisting of nonsquamous epithelial and submucosal layers was included (Figure B1).

The following equation governs mass balance in the air phase of the nasal vestibule, where a simplified mass transfer term on squamous epithelium was implemented at the air:tissue interface:

$$V_s \frac{dC_s}{dt} = Q_a(C_{in} - C_s) - K_s C_s \qquad [B1]$$

where V_s is the volume of the air phase of the nasal vestibule, Q_a is the inhalation airflow rate, C_{in} is the inhalation concentration, C_s is the air phase concentration, and K_s is the mass transfer coefficient (see text for derivation of K_s).

The following equations govern mass balance in the remaining compartments:

Air:

$$V_a \frac{dC_a}{dt} = Q_a(C_s - C_a) - k_g S_t(C_a - C_t/P_{t:a}) \qquad [B2]$$

Epithelium:

$$V_t \frac{dC_t}{dt} = k_g S_t(C_a - C_t/P_{t:a}) - k_b S_b(C_t - C_b/P_{t:b}) - k_f V_t C_t - \frac{V_{\max} \cdot C_t}{K_m + C_t} \qquad [B3]$$

Submucosal:

$$V_b \frac{dC_b}{dt} = k_b S_b(C_t - C_b/P_{b:t}) - k_f V_b C_b - \frac{V_{\max} \cdot C_b}{K_m + C_b} - Q_b C_b \qquad [B4]$$

where C_a, C_t, *and* C_b are the concentrations in air, tissue, and submucosa, respectively; V_a, V_t, *and* V_b are the air, tissue, and submucosal volumes; and Q_a and Q_b are the air and blood flow rates. The mass transfer coefficients k_g and k_b govern diffusion rates into tissue and blood, respectively. The air-phase mass transfer coefficient, k_g, was obtained from previous CFD simulations (Jarabek et al., 2001) using a $C = 0$ boundary condition in a zonal approach for the rat nose. This involved coronally dividing the CFD model of the rat nose into 12 zones and calculating the fractional penetration of inhaled gas in each zone. The zones were sequentially made nonabsorbing anterior to the zone of interest, and completely absorbing in the posterior direction toward the nasopharynx, to ensure that an accurate mass transfer could be computed in the distal regions of the nose. Tissue phase resistance was disregarded so that the total resistance consisted only of the resistance to mass transfer in the air phase. Mass transfer coefficients were computed in each zone and combined into a single mass transfer coefficient for the entire rat nose. Values for k_g were 1.5 and 2.5 cm/s for inhalatory flow rates of 148 and 443 ml/min, respectively. The liquid-phase mass transfer coefficient was defined as $k_b = D_b/L_b$ to describe mass transfer through the submucosal layer by diffusion.

Equations (B1)–(B4) were solved for nasal extraction (NE), given as percent of mass absorbed in the nose:

$$NE = 100 \cdot \frac{C_{in} - C_a}{C_{in}}$$

The first-order rate constant, k_f, and the Michaelis–Menten parameters $V_{\max}$ and K_m were estimated by fitting predicted NE to time-averaged nasal extraction data.

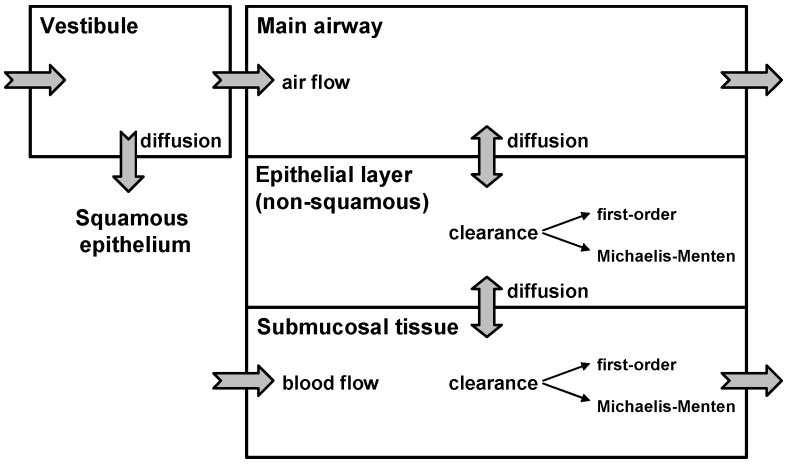

FIG. B1. Schematic of the PK model of the rat nose simulating steady-state inspiratory airflow and gas uptake in squamous and nonsquamous epithelium. The PK model provided a simple compartmental representation of the rat nasal CFD model that can be easily used for parameter optimization.